

Electrochemical Stability of $\text{Li}_{10}\text{GeP}_2\text{S}_{12}$ and $\text{Li}_7\text{La}_3\text{Zr}_2\text{O}_{12}$ Solid Electrolytes

Fudong Han, Yizhou Zhu, Xingfeng He, Yifei Mo,* and Chunsheng Wang*

The electrochemical stability window of solid electrolyte is overestimated by the conventional experimental method using a Li/electrolyte/inert metal semi-blocking electrode because of the limited contact area between solid electrolyte and inert metal. Since the battery is cycled in the overestimated stability window, the decomposition of the solid electrolyte at the interfaces occurs but has been ignored as a cause for high interfacial resistances in previous studies, limiting the performance improvement of the bulk-type solid-state battery despite the decades of research efforts. Thus, there is an urgent need to identify the intrinsic stability window of the solid electrolyte. The thermodynamic electrochemical stability window of solid electrolytes is calculated using first principles computation methods, and an experimental method is developed to measure the intrinsic electrochemical stability window of solid electrolytes using a Li/electrolyte/electrolyte-carbon cell. The most promising solid electrolytes, $\text{Li}_{10}\text{GeP}_2\text{S}_{12}$ and cubic Li-garnet $\text{Li}_7\text{La}_3\text{Zr}_2\text{O}_{12}$, are chosen as the model materials for sulfide and oxide solid electrolytes, respectively. The results provide valuable insights to address the most challenging problems of the interfacial stability and resistance in high-performance solid-state batteries.

electrochemical stability window, and (3) chemical compatibility with the anode and cathode. In the past few years, major advances have been achieved in increasing the Li ionic conductivity of the solid electrolytes. The state-of-the-art solid electrolyte materials, such as Li-garnet $\text{Li}_7\text{La}_3\text{Zr}_2\text{O}_{12}$ (LLZO) and $\text{Li}_{10}\text{GeP}_2\text{S}_{12}$ (LGPS) have achieved an ionic conductivity of 10^{-3} to 10^{-2} S cm^{-1} ,^[1,2] which are comparable to commercial organic liquid electrolytes. The high ionic conductivity in solid electrolytes has ignited the research of all-solid-state Li-ion batteries. After achieving adequate Li ionic conductivity in the solid electrolyte materials, current research efforts turned to enhancing the electrochemical stability of the solid electrolytes and chemical compatibility between the solid electrolytes and electrodes, so that Li metal anode and high voltage cathode materials can achieve higher energy density in all-solid-state Li-ion batteries.

1. Introduction

The safety issue of Li-ion batteries has resulted in fire incidences for electric vehicles and airplanes. The use of flammable organic electrolytes in commercial Li-ion batteries is often blamed. Replacing the organic electrolyte with inorganic, ceramic solid electrolytes, which are intrinsically nonflammable, to assemble all-solid-state Li-ion batteries has the promise to ultimately resolve the safety issue of Li-ion batteries. Similar to an organic liquid electrolyte, a solid electrolyte has also to satisfy three critical requirements: (1) high Li ionic conductivity of $>10^{-3}$ S cm^{-1} and low electronic conductivity, (2) wide

To enable the highest voltage output of the solid-state battery by coupling a lithium metal anode with a high voltage cathode material, a very wide electrochemical stability window (0.0–5.0 V) is desired for an ideal solid electrolyte. The electrochemical stability window of solid electrolyte was typically obtained by applying the linear polarization on the Li/solid electrolyte/inert metal (e.g., Pt) semiblocking electrode. Tested by this method, very wide electrochemical stability windows of 0.0 to 5.0 V were reported for both LGPS and LLZO.^[2,3] However, the electrochemical performances of the bulk-type all-solid-state battery batteries assembled with these solid electrolytes^[2,4] are far worse than the liquid-electrolyte based batteries even though the solid electrolyte has a comparable ionic conductivity to the liquid electrolyte. The high interfacial resistance is often blamed as the main limiting factor for the performance of the solid state battery.^[5] The origin of the interfacial resistance, though still not fully understood, is often attributed to the poor physical interfacial contact, the formation of space charge layers,^[6] and/or the formation of interphase layers due to the chemical reactions between the electrolyte and electrode.^[7] Although a variety of interfacial processing techniques, such as dynamic pressing,^[8] nanosizing,^[9] cosintering,^[10] screen printing,^[11] surface coatings^[12,13] have been attempted to engineer the interfaces between the electrodes and electrolytes, the performances of the solid-state battery are still much lower than the liquid-electrolyte based batteries. The limited electrochemical stability

F. Han, Prof. C. Wang
Department of Chemical and Biomolecular
Engineering
University of Maryland
College Park, MD 20742, USA
E-mail: cswang@umd.edu

Y. Zhu, X. He, Prof. Y. Mo
Department of Materials Science and Engineering
University of Maryland
College Park, MD 20742, USA
E-mail: yfmo@umd.edu



DOI: 10.1002/aenm.201501590

of the solid electrolyte is rarely thought to be an issue, since the batteries are cycled within the “wide” stability window of electrolytes measured using the semiblocking electrode.^[14]

However, recent studies have challenged the claimed stability of the solid electrolyte materials. For example, LiPON, a solid electrolyte demonstrated to be compatible with Li metal anode, has recently been shown to decompose against Li metal.^[15] In addition, our first principles computational and experimental study demonstrated the reversible reduction and oxidation of the LGPS solid electrolyte materials at 0–1.7 V and 2–2.5 V, respectively,^[5] which indicated a true electrochemical window of the LGPS significantly narrower than the 0.0–5.0 V window obtained using the semiblocking electrode.^[5,16] These results suggest that the electrochemical window measurements based on the semiblocking electrodes significantly overestimated the true electrochemical window governed by the intrinsic thermodynamics of the material. The overestimated electrochemical stability of solid electrolytes is caused by the slow kinetics of the decomposition reactions due to the small contact area between LGPS and current collectors.^[5] However, in the bulk-type all-solid-state battery, a large amount of carbon and solid electrolyte are mixed together with the active materials to form the composite electrode.^[9,10] As a result, the reduction or oxidation kinetics of the solid electrolyte in the composite electrode is significantly accelerated because of the significantly-increased contact area between the solid electrolyte and electronic conductive additives. The electrochemical stability window of the electrolyte in the carbon-electrolyte-active material electrode composite cannot be properly captured by the semiblock electrodes, which may be only more suitable for the cell configurations in thin-film solid-state batteries.^[17] Therefore, a proper cell design is needed to evaluate the electrochemical window of the solid electrolyte in the bulk-type all-solid-state batteries.

More importantly, the limited stability of the solid electrolyte materials, though still neglected by battery community, has significantly restricted the performance of all-solid-state Li-ion batteries. At the cycling voltages beyond the stability window of the solid electrolyte, the decomposition products of the solid electrolyte would form as an interphase at the interfaces between solid electrolyte and electronic conductive additives. Depending on the properties of the decomposition products, the interphase may lead to an increase in interfacial resistances and a decrease in the performance of the bulk-type solid-state battery. Unfortunately, the interfacial resistance arising from the decomposition of solid electrolytes has been ignored so far due to the overestimated stability window from the semiblocking electrode measurements. The intrinsic (true) electrochemical stability window of solid electrolytes is critical in understanding the origins of high interfacial resistance in the bulk-type solid-state Li-ion batteries. However, only few theoretical studies have examined the electrochemical stability of solid electrolytes, and no existing experimental technique can measure the true stability window of the solid electrolytes.

In this study, we challenge the claimed stability of the solid electrolyte materials and the use of semiblock electrode design for evaluating the electrochemical window for solid electrolyte materials. The most promising solid electrolytes, Li₁₀GeP₂S₁₂ and cubic Li-garnet Li₇La₃Zr₂O₁₂, were chosen as the model materials for sulfide and oxide solid electrolytes, respectively.

First principles calculations were performed to obtain the intrinsic thermodynamic electrochemical stability windows. A new Li/electrolyte/electrolyte-carbon cell was proposed to replace current Li/electrolyte/Pt semiblocking electrode for the measurement of the true electrochemical stability window of solid electrolytes. The first principles computation and experimental results are in good agreement, indicating that both of these solid electrolyte materials have narrower electrochemical window than what was previously claimed. The understanding of the intrinsic thermodynamics about the solid electrolyte materials at different voltages during the battery cycling provides invaluable guidance for the development of the bulk-type all-solid-state battery.

2. Results

2.1. Electrochemical Stability of Li₁₀GeP₂S₁₂

Lithium sulfide-based solid electrolytes exhibit high ionic conductivity, low grain boundary resistance, and the excellent mechanical property, which allows forming a good interfacial contact with the electrode by cold-pressing without high temperature sintering.^[18,19] In this study, Li₁₀GeP₂S₁₂ (LGPS) is chosen as a typical example of sulfide electrolytes. LGPS was reported to have the highest room-temperature ionic conductivity ($\approx 10^{-2}$ S cm⁻¹)^[2] among all solid electrolyte materials and a wide “apparent” electrochemical stability window of 0.0–5.0 V determined by cyclic voltammetry of a Li/LGPS/Pt semiblock electrode.^[2]

However, the first principles computation using Li grand potential phase diagram demonstrated that the intrinsic stability window is much narrower than 0.0–5.0 V.^[16] The Li grand potential phase diagram identifies the phase equilibria at different potentials and the most thermodynamically favorable reactions at the given potential, assuming the full thermodynamic equilibrium and no kinetic limitation in the reaction and transportation. The same computation scheme has been used in the calculations of voltages and reaction energies in the lithiation/delithiation of battery materials. **Figure 1** shows the calculated voltage profile and phase equilibria of LGPS upon lithiation and delithiation, confirming that LGPS has a much narrower electrochemical window than 5.0 V.^[2] The reduction of the LGPS starts at 1.71 V, where LGPS is lithiated and turns into Li₄GeS₄, P, and Li₂S. With further decrease of the potential, there are multiple thermodynamic voltage plateaus corresponding to the Li-P and Li-Ge alloying processes upon lithiation. Our calculations predicted the reduction products of LGPS to be Li₂S, Li₁₅Ge₄, Li₃P at 0 V, which have been confirmed by the experimental results.^[5] On the other hand, the oxidation of the LGPS to Li₃PS₄, S, and GeS₂ starts at only 2.14 V, and the formed Li₃PS₄ is further oxidized into S and P₂S₅ at 2.31 V. In summary, our calculation results have shown that the LGPS has a limited electrochemical stability window from 1.7 to 2.1 V.

Cyclic voltammetry (CV) was used to experimentally evaluate the electrochemical stability of LGPS. Using the conventional Li/LGPS/Pt semiblocking electrode (voltage range: –0.6 to 5.0 V), the decomposition current within the voltage window of 0.0 to 5.0 V cannot be observed from the CV of LGPS.^[2,5]

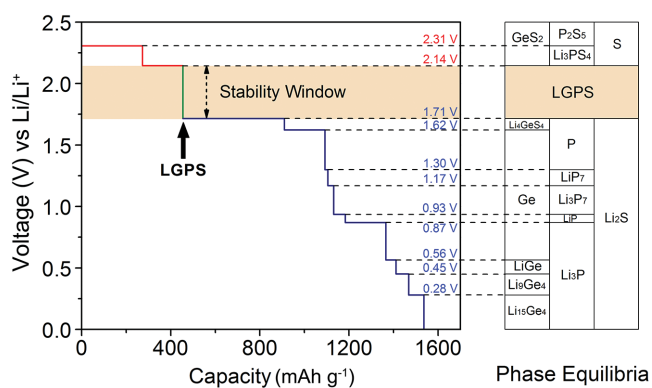


Figure 1. The first principles calculation results of the voltage profile and phase equilibria of LGPS solid electrolyte upon lithiation and delithiation.

The “wide” electrochemical stability window of 0.0–5.0 V is because the decomposition current is very small and is underestimated by the huge Li deposition/dissolution peaks.^[20] To avoid the huge Li deposition/dissolution peaks, the conventional Li/LGPS/Pt semiblocking electrode was scanned within restricted voltage windows (0.0–2.5 V and 2.5–4.0 V). As shown in Figure S1 (Supporting Information), apparent current due to the decomposition of LGPS could be clearly observed in the linear scan of the Li/LGPS/Pt although the reaction current is still very low due to the limited interfacial contact between LGPS and Pt in the Li/LGPS/Pt cell. In this regard, we propose a novel experimental method to measure the electrochemical stability window of LGPS using a Li/LGPS/LGPS-C/Pt cell. A large amount of carbon (graphite, KS-4) was mixed into LGPS (weight ratio of LGPS to carbon is 75:25) to form the electrode. The increased contact between LGPS and carbon would significantly improve the kinetics of the decomposition reaction due to the facile electron transport as well as the significantly increased active area for charge-transfer reaction. Thus, the intrinsic stability window of LGPS is expected to be obtained from the CV scan of the Li/LGPS/LGPS-C/Pt cell. Since the electrochemical decomposition and the lithiation/delithiation of the LGPS are essentially the same process but described from two different perspectives, the reversible decomposition of LGPS electrolyte had been demonstrated using the same Li/LGPS/LGPS-C/Pt cell in Figure S2 in the Supporting Information^[5] of our previous work. The result indicates that the reduction of LGPS starts at 1.7 V while the oxidation of LGPS starts at 2.1 V. This electrochemical behavior agrees very well with the computational results, and both computational and experimental results indicate the true electrochemical stability window of 1.7 to 2.1 V for LGPS. Additionally, the oxidation of S at high potentials and the formation of Li-Ge and Li-P alloys at the low potentials were also confirmed by the X-ray photoelectron spectrum results.^[5] The main function of carbon in the LGPS-C composite is to increase the electronic conductivity of LGPS so that the decomposition kinetics could be improved. In this regard, carbon is not the only option for the electronic-conductive additive. To exclude the potential interactions between carbon and LGPS, we replaced carbon with the inert metal powder (Pt black), i.e., 25 wt% Pt black and mixed Pt with LGPS to form the LGPS-Pt composite electrode. The CV curves of the

Li/LGPS/LGPS-Pt/Pt cell are shown in Figure S2 (Supporting Information). Both the oxidation and reduction peaks could be observed at similar voltages in the CV curves of the Li/LGPS/LGPS-C/Pt cell. The result implies that the redox peaks in Li/LGPS/LGPS-C/Pt cell is not induced by the reaction between carbon and LGPS but the decomposition of LGPS itself. These results demonstrated that the thermodynamic electrochemical stability window of LGPS can be accurately calculated using our computation scheme, and that Li/LGPS/LGPS-C/Pt cell can be used to measure the true electrochemical stability of LGPS.

Therefore, our proposed method of measuring the electrochemical stability of the electrolyte in Li/electrolyte/electrolyte-C cell is demonstrated to obtain the “true” electrochemical stability window based on the intrinsic thermodynamics of the solid electrolyte. The Li/electrolyte/electrolyte-C cell provides improved kinetics from large and continuous physical contacts between solid electrolyte and carbon to facilitate the thermodynamically favorable decomposition reactions of the solid electrolyte. The kinetics of these reactions is limited in the semiblocking electrode, which yields overestimated electrochemical stability. Moreover, the use of the Li/electrolyte/electrolyte-C cell mimics the cell configuration in the bulk-type solid-state battery and represents the real microstructural architectures in the solid-state electrode composite, where carbon and solid electrolyte are mixed with the active material. It should be noted that in this work we mainly focused on the thermodynamic electrochemical stability of the solid electrolyte materials. The degree (extent) of the decomposition of a solid electrolyte depends on the kinetics of decomposition reaction. The particle size of solid electrolyte, the electronic and ionic conductivities of electrolyte-carbon composite, the electronic and ionic conductivities of decomposition products, and the applied current (or CV scan rate) all change the reaction kinetics, thus the degree of decomposition of solid electrolyte. The passivation from the electronic insulating decomposition products may also prevent further decomposition of solid electrolyte. These indicate that the decomposition of the solid electrolyte in the real all-solid-state cell may not be as severe as that in the Li/electrolyte/electrolyte-C cell because of the low content of carbon in the electrode composite. However, even a slight amount of decomposition of the solid electrolyte may cause a huge interfacial resistance in the real cell, which was always ignored and will be discussed in detail in Section 3. Therefore, the measurements based on the Li/electrolyte/electrolyte-C cell could help to understand the electrochemical interfacial behavior of the solid electrolyte in the real bulk-type solid-state battery.

In addition, we calculated the electrochemical stability of other sulfide electrolytes, such as $\text{Li}_{3.25}\text{Ge}_{0.25}\text{P}_{0.75}\text{S}_4$, Li_3PS_4 , Li_4GeS_4 , $\text{Li}_6\text{PS}_5\text{Cl}$, and $\text{Li}_7\text{P}_2\text{S}_8\text{I}$, using the same computation scheme.^[21] The thermodynamically intrinsic electrochemical stability windows and the decomposition phase equilibria beyond their stability window are very similar to those of LGPS. The cathodic limit is around 1.6–1.7 V for the reduction of Ge or P contained in the sulfide electrolytes, and the anodic limit is usually around 2.1–2.3 V corresponding to the oxidization of S. Doping halogen elements, such as Cl and I, into the materials increases the potential to fully delithiate the materials.^[22–24] The results indicate that the narrow electrochemical stability window is originated from the reduction of P/Ge and the oxidization of S.

2.2. Electrochemical Stability of $\text{Li}_7\text{La}_3\text{Zr}_2\text{O}_{12}$

Despite the high ionic conductivity, most of the sulfide electrolytes are sensitive to moisture and/or oxygen in the ambient environment. The oxide-based solid electrolytes, which have better stability in air, therefore attract a lot of interests. In particular, cubic Li-stuffed garnet (i.e., $\text{Li}_7\text{La}_3\text{Zr}_2\text{O}_{12}$) reported with a wide electrochemical stability window of 0.0–6.0 V^[3,25] and a high ionic conductivity of 10^{-4} – 10^{-3} S cm^{-1} ,^[1] is considered as one of the most promising oxide solid electrolytes. In this section, the same research methodology was applied to study the electrochemical stability window of lithium oxide-based solid electrolyte, especially LLZO.

The voltage profile of LLZO upon lithiation/delithiation and the detailed phase equilibria of LLZO at different voltages were calculated using the first principles method (Figure 2). The results show that the thermodynamic electrochemical stability window of LLZO is also smaller than the reported value of 0.0–6.0 V.^[3] The oxidation decomposition of LLZO occurs at as low as 2.91 V to form Li_2O , $\text{Li}_6\text{Zr}_2\text{O}_7$, and La_2O_3 . As the voltage increases above 3.3 V, O_2 is generated from the oxidation of Li_2O_2 (Figure 2). At below 0.05 V, LLZO is lithiated and reduced into Li_2O , Zr_3O , and La_2O_3 , and Zr_3O may be further reduced into Zr metal at below 0.004 V (Figure 2). The thermodynamic results based on the energetics of DFT calculations indicate LLZO is not thermodynamically stable against Li metal. However, the reduction potential of LLZO (0.05 V) is very close to Li metal deposition potential (0 V), the thermodynamic driving force for the reduction is very small. Since these values of energy and voltage (0.004 V) for the further reduction of Zr_3O are as small as the potential errors of typical DFT calculations and the approximations in our calculation scheme, the exact potential to reduce Zr_3O into Zr may be below or above 0 V. However, if the potential is significantly lower than 0 V, the formation of Zr would be thermodynamically favorable. In addition, we also evaluated the electrochemical stability of the garnet phases doped by the cation dopants, such as Ta, Nb, and Al (Tables S1–S3, Supporting Information), which are commonly applied to stabilize the cubic phase of LLZO and to increase the Li ionic conductivity. The calculations indicate that a small amount of dopants, such as Ta, Al, Nb, which may be reduced at a slightly higher reduction potential, does not have

a large effect on the reduction/oxidation of the host elements in LLZO (Tables S1–S3, Supporting Information). At 0.0 V, the doped cations Ta and Nb are reduced into metallic states, and Al is reduced into Zr–Al alloys. Considering the low amount of dopants in LLZO, the effects of dopants on the stability window are small. Given the low reduction potentials for the garnet reduction, the good stability of the garnet LLZO may be explained by the formation of surface passivation after decomposition, such as Li_2O , La_2O_3 , and other oxides. In addition, the formation of Li_2CO_3 surface layers due to reaction of LLZO with the CO_2 in the air may also help passivating the LLZO.^[26,27] These results may explain why LLZO was widely observed to be stable with Li at room temperature in many studies.^[25,28]

The CV of the Li/LLZO/LLZO-C/Pt cell was used to measure the electrochemical stability window of LLZO, which was doped with a small amount of Ta to stabilize the cubic phase of LLZO.^[29] To increase the contact area between the LLZO and carbon, the as-obtained LLZO powder was ground using a high-energy ball mill to reduce its particle size below 1 μm , and then a thin-layer of carbon was coated on LLZO, as shown in Figure S3 (Supporting Information). The carbon-coated LLZO was then mixed with carbon black (weight ratio is 40:60) to make the LLZO-C composite electrode. All these processes were done in an Ar atmosphere to protect the LLZO from the slow reaction with the $\text{H}_2\text{O}/\text{CO}_2$ in air.^[26,27] The XRD test (Figure S4, Supporting Information) confirmed that the LLZO structure remained after grinding and carbon-coating processing. The same Zr 3d spectra of LLZO before and after carbon coating (Figure S5, Supporting Information) indicates that LLZO is stable upon high-temperature carbonization process and no apparent carbothermal reduction of Zr could be observed. The thermodynamic oxidation stability of the LLZO was examined by the CV scan of the Li/LLZO/LLZO-C cell within the voltage range of 2.6–10.0 V. As can be observed from Figure 3, the apparent oxidation of LLZO starts at about 4.0 V, which is much lower than the reported value of 6.0 V. The subsequent cathodic scan indicates the oxidation reaction is not reversible, and no oxidation peak can be observed in the second cycle. The maximum current of ≈ 5 μA in Figure 3 indicates that only a small amount of LLZO was oxidized. It should also be noted that the small oxidation current could also come from the insufficient ionic conduction in the LLZO-C composite because of the large amount of carbon additives as well as the large grain boundary resistance between LLZO particles. A larger current would be expected if a continuous ionic pathway through LLZO was formed in the LLZO-C composite (e.g., from co-sintering of LLZO solid electrolyte and LLZO-C electrode.^[10]) The higher voltage (4.0 V) compared with the calculation result (2.91 V) can be explained by the large over-potential for the oxidation of LLZO. It should be noted that the CV scan of Li/LLZO/LLZO-C/Pt cell was tested in an Ar-filled glovebox and similar results were obtained when graphite was used as the electronic conductive additive, excluding the oxidation of carbon additives if LLZO is stable. Since the reduction potential of the LLZO at 0.05 V is very close to the voltage of Li metal, it is difficult to distinguish the reduction of LLZO from the Li deposition in the CV scan and to quantify the reduction potential of LLZO.

X-ray photoelectron spectroscopy (XPS) was used to identify the reduction and oxidation products of LLZO beyond its

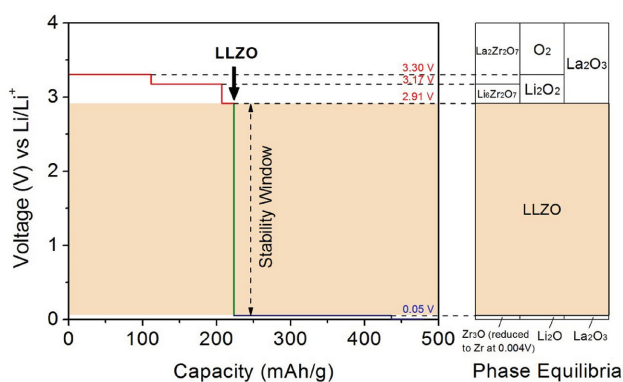


Figure 2. The first principles calculation results of the voltage profile of LLZO solid electrolyte upon lithiation and delithiation.

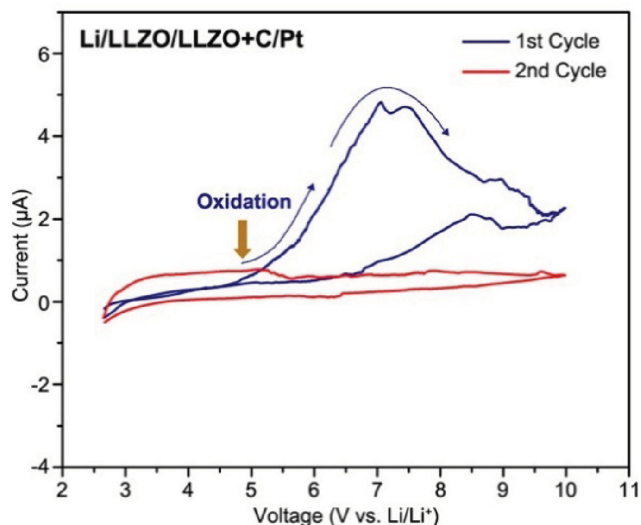


Figure 3. Cyclic voltammetry of Li/LLZO/LLZO-C/Pt cell within the voltage range of 2.6–10.0 V.

stability window. In order to increase the yields of decomposition products for characterization, the LLZO-C composite electrode was cycled against Li metal in a liquid electrolyte, which provided faster reaction kinetics. A 5-V class liquid electrolyte, 1 M LiPF₆ in a mixed solvent of FEC, FEMC, and HFE (volume ratio is 2:6:2), was used to minimize the oxidation from the liquid electrolyte. The Li/LLZO half-cells were charged to 4.5 V or discharged to 0 V at a current density of 10 mA g⁻¹ and were then maintained at the voltages for 72 h. The charge and discharge curves of the LLZO-C composite electrodes are provided in the Supporting Information (Figure S6, Supporting Information). However, it is impossible to conclude the decomposition of the LLZO simply from the charge/discharge curve of the LLZO-C electrode in Figure S7 (Supporting Information) because carbon in the LLZO-C electrode will also react with lithium and solid-electrolyte-interphase (SEI) is also formed on carbon.

Therefore, XPS was used to characterize the decomposition of LLZO. Figure 4a shows the XPS survey of the fresh and charged LLZO electrodes. The atomic percentages of the O and Zr derived from the survey (Table 1) indicates the atomic ratio of O to Zr decreases from 7.6:1 to 4.9:1 after LLZO was charged to 4.5 V. It should be noted that 2h Ar⁺ sputtering was performed on the surface of the charged LLZO before collecting the atomic concentrations of O and Zr in order to completely remove the surface layers caused by the decomposition of the liquid electrolyte at a high potential. The complete removal of SEI after sputtering is confirmed by the XPS spectra of C 1s of the LLZO-C samples upon different sputtering times (Figure S7, Supporting Information). Multiple peaks above 284.6 eV (carbon black) could be observed for the charged LLZO before sputtering, indicating that several carbon-containing species are present at the surface. These carbon-containing species are most likely attributed to the decomposition products of the liquid electrolyte. However, after 1 h sputtering, only one peak at 284.6 eV corresponding to the carbon black in the LLZO-C electrode could be observed in the sample, which means that all the SEI species were removed. One more hour sputtering was performed in order to completely remove the surface layer. This result confirms that O₂ was released from the charged LLZO, which is consistent with our computation result (Figure 2). No obvious binding energy shift can be observed for Li, La, Zr, O elements after the LLZO was charged. On the other hand, Figure 4b compares the high-resolution spectra of Zr 3d of LLZO electrodes at the fresh and discharged states. All Zr 3d spectra exhibit a doublet with a fixed difference of 2.43 eV because of the spin-split coupling between 3d_{5/2} and 3d_{3/2}. For the fresh LLZO electrode, two different chemical environments of the Zr can be observed. The main peak of Zr 3d_{5/2} located at the 181.8 eV corresponds to the Zr in the cubic garnet,^[26] while the side peak of the Zr 3d_{5/2} at the 179.7 eV may be ascribed to the oxide impurities (e.g., La₂Zr₂O₇) at the surface of the sample though the amount of the impurities is too small to be detected in the XRD test.^[30,31] Both Zr peaks remained with the increased relative intensity of the side peak at 179.7 eV, after the LLZO was

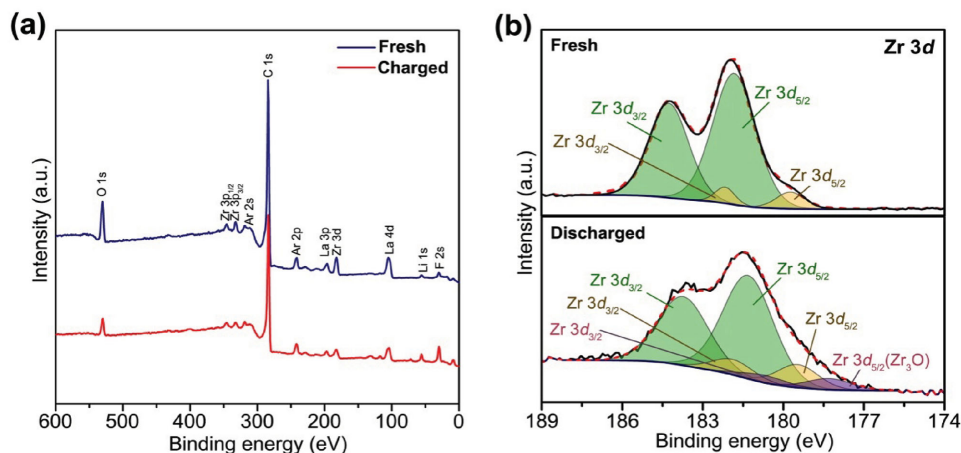


Figure 4. a) The XPS survey spectrum of the fresh and charged LLZO. The atomic percentage of O and Zr in the sample is obtained from the area of O 1s and Zr 3d peak, respectively. b) High resolution Zr 3d core XPS spectra of fresh and discharged LLZO. The curve fits were obtained using fixed spin splits ($3d_{3/2} - 3d_{5/2} = 2.43$ eV).

Table 1. XPS analysis-derived O and Zr elements atomic concentrations.

Samples	O content [at%]	Zr content [at%]	O/Zr ratio
Fresh	6.64	0.87	7.6:1
Charged to 4.5 V	2.12	0.43	4.9:1

discharged to 0 V. In addition, another peak at a lower binding energy of 178.2 eV also appears for the discharged LLZO. It is known that various Zr suboxides exist and their binding energy will shift to a lower value as the oxidation state of Zr decreases.^[32] The increase in the relative intensity of side peak at 179.7 eV as well as the appearance of a new peak at a lower binding energy (178.2 eV, ascribed to Zr₃O herein) confirmed the reduction of Zr in the discharged LLZO, which agrees with the calculation result. It should be noted that the main peak at 181.8 eV of Zr still remained after the LLZO was discharged to 0 V, indicating that only the surface of the LLZO was reduced and most of LLZO was still stable. Nevertheless, our results demonstrated that the electrochemical stability window of garnet is not as wide as previously reported, and the reduction of Zr and the oxidation of O contained in LLZO occur beyond the stability window of LLZO.

Our computation and experimental results provide a new mechanism for the short-circuiting across the Li/LLZO/Li cell during Li stripping/plating test at a high overpotential.^[33–35] It was reported that the Li dendrite growth across the LLZO electrolyte layer is responsible for the short circuiting of Li/LLZO/Li electrolyte cell. However, the growth of soft, ductile Li dendrite through the hard, dense layer of the LLZO is not understood. Here, we propose an alternative mechanism on the basis of the reduction of LLZO at very large overpotentials. As a result of the cation reduction, the formation of metallic states at the interfaces of the Li-LLZO and of the LLZO grain boundaries facilitates the electronic conduction at these interfaces. The electronic conduction would facilitate the deposition of Li in the materials from the Li electrode or the Li ions in the garnet materials. In addition, the coloration of the LLZO surface from tan white to gray black was observed after LLZO was immersed in molten Li (300 °C) for 168 h.^[36] We believe that the coloration is related to the reduction of Zr and/or the dopant (Al) in LLZO. The undetected oxidation change of Zr in their XPS result^[36] may be caused by the re-oxidation of the top-surface of the sample stored in dry room, since the surface of Zr is very sensitive to oxygen and will be gradually oxidized to ZrO₂ after long time exposure of air.^[32]

The thermodynamic electrochemical stability windows and the decomposition phase equilibria at different voltages of other common oxide solid electrolytes were also calculated.^[21] The oxide solid electrolytes generally have a wider stability window than sulfides. The stability window of oxide solid electrolyte varies significantly from one material to another. Li-garnet LLZO has the lowest cathodic limit of 0.05 V, suggesting the best resistance to reduction. The NASICON-type materials, Li_{1.3}Al_{0.3}Ti_{1.7}(PO₄)₃ (LATP) and Li_{1.5}Al_{0.5}Ge_{1.5}(PO₄)₃ (LAGP), have the highest reduction potential of 1.7 and 2.2 V, respectively, and also have the highest oxidation potential of ≈4.2 V. We found that the anodic limit of the electrolyte is related with the oxidation of the O in the compounds. The reduction of Ge,

Ti, P, Zn, and Al elements contained in the solid electrolytes is generally responsible for the cathodic limit.

3. Discussions

Our first principles computation and experimental results indicate most solid electrolytes, especially sulfides, have an intrinsically narrower electrochemical stability window than the “apparent” window obtained from the linear scan of semi-blocking electrode. No solid electrolyte is thermodynamically stable over the wide range from 0.0 to 5.0 V. Therefore, most electrolytes are not stable within the cycling voltage range of typical Li-ion battery cells based on the lithium anode and LiCoO₂ cathode. The main problem for operating the solid electrolyte beyond the limited thermodynamic stability window is the formation of new interphases due to the decomposition at the active material-electrolyte and carbon-electrolyte interfaces. The decomposition interphases, which likely have poorer Li ion conductivity than the solid electrolyte, would impede the Li transport between the solid electrolyte and the active materials and would increase the interfacial resistance. Therefore, the performance of the bulk-type solid-state battery is greatly affected, depending on the properties of the decomposition interphases, such as ionic conductivity, electronic conductivity, and electrochemical reversibility.

The most desired properties of the interphases are electrochemically irreversible, highly ionic conducting but electronic insulating. The interphase with such properties is essentially the SEI, which kinetically inhibit further decompositions of solid electrolyte and extend the electrochemical window. The formation of the SEI layer is similar to that on the graphite electrode in the commercialized lithium ion battery, which enabled the liquid electrolyte to be used beyond its stability window.^[14] For example, the decomposition products of Li₂O, Li₃N, and Li₃P formed at the reduction and lithiation of LiPON serve as an excellent SEI,^[15] enabling its stability with Li metal for extremely long charge/discharge cycles.^[17] In addition, Li₃N and Li₃P are good Li ionic conductor materials, which lower the interfacial resistance.^[37,38] However, it is more likely to have the interphase with lower Li ionic conductivity than the original electrolyte, causing high interfacial resistance at the interface. Even worse, the interphase would be highly detrimental if the decomposition products have sufficient electronic conductivity. In this case, the decomposition of the solid electrolyte would continue into the bulk of the solid electrolyte, eventually causing short circuiting of the battery. For example, the well-known reduction of the LLTO is due to the high electronic conductivity of LLTO after the reduction of Ti at low potentials.^[39] The formation of metals or metal alloys at reduction, which is typical for the solid electrolytes containing certain cations, such as Ge, Ti, Zn, and Al, prevents the formation of SEI layers. For such solid electrolyte materials, an artificial SEI layer is required to be inserted at the electrode/electrolyte interface to passivate the solid electrolyte and to suppress the decomposition of the solid electrolyte beyond its stability window.

In addition, it is highly undesired to have reversible or partially reversible decomposition reactions during lithiation/delithiation, which make the electrolyte essentially an active

electrode.^[39,40] The decomposition of the electrolyte at the interfaces would reduce the electrolyte content in the electrode composite, and the repeated volume changes during the cycling may lead to the poor physical contacts at the interfaces of the electrolyte. For example, the oxidation products of sulfide electrolytes at high voltages contain S, which is a well-known cathode material in Li-S batteries. The lithiation/delithiation of S at the interfaces of LGPS-cathode and LGPS-carbon interfaces generates a large volume change of up to 180% at the interface.^[41] In addition, the changes of electronic and ionic conductivities in the interphase upon lithiation/delithiation would also affect the interfacial resistances and performance of the solid state batteries during cycling. The EIS test of the Li/LGPS/LGPS-C cells at different voltages (Figures S8 and S9, Supporting Information) confirmed that oxidation and reduction decomposition of LGPS will increase the interfacial resistance of the cells.

To avoid the undesirable decompositions of the solid electrolyte, one strategy is to limit the voltage of the battery to suppress the formation of detrimental decomposition products. For example, the decomposition of LLZO will be intrinsically avoided if we use Li-In alloy as an anode (0.6 V) and S as a cathode (2.3 V). In addition, Li-In anode is widely used for the sulfide solid electrolytes, because the Li-In alloying potential higher than the reduction of Ge suppresses the Li-Ge alloying and further decompositions in the sulfide solid electrolytes. However, the use of Li-In anode significantly decreases the capacity and voltage of the battery. Another strategy to extend the stability of the solid electrolyte is to apply the coating layers at the electrolyte–electrode interfaces, since the choice of the materials is very limited to simultaneously satisfy all battery criteria (e.g., voltage, capacity, and chemical compatibility).^[21] For example, the artificial coating layer, such as $\text{Li}_4\text{Ti}_5\text{O}_{12}$ and LiNbO_3 , has been applied at the interface between the sulfide solid electrolyte and cathode materials.^[12,42] These coating layers are found to suppress the interfacial mutual diffusion and to reduce the interfacial resistance. In addition, the formation of Li_2CO_3 on the surface of LLZO after exposing to air^[26,27] can be considered as a SEI, which protects the reduction of LLZO against Li. At the anode side, Polyplus has applied the coating layers to stabilize the LATP materials against Li metal anode.^[43] The above examples suggest the formation and coating of the SEI-like layers is an effective strategy to extend the stability window of the solid electrolyte and to improve the performance of all-solid-state batteries.

On the basis of our new understanding, we provide specific recommendations for the engineering of sulfides and oxides solid electrolyte materials in the all-solid-state batteries. Since LGPS has a limited electrochemical stability window with a reduction potential of 1.7 V and an oxidation potential of 2.1 V, the anode materials, such as In, with the lithiation potential higher than Li-Ge alloying is recommended for LGPS electrolyte to avoid the formation of highly electronic conductive Li-Ge alloys. The problems of the LGPS solid electrolyte at the cathode side is that the oxidation products, P_2S_5 , S, and GeS_2 are neither electronic nor ionic conductive, and that the oxidation product S is electrochemically reversible if mixed with carbon. Therefore, applying an artificial SEI layer is recommended at the interface between the high voltage cathode and LGPS to provide good battery performance. LLZO has a wider

electrochemical window than LGPS. In particular, LLZO holds great promises for the application with lithium metal anode, because the stability of LLZO against Li metal can be easily circumvented by kinetic protections, given the very small thermodynamic driving force for the reduction of LLZO at 0 V. Such kinetic protections should be able to sustain large current densities and high temperatures, which would facilitate the Li reduction of LLZO, during the operation of the LLZO-based batteries. At the cathode side, the stability of the LLZO may not be an issue as the oxidation products consisting electronic insulating $\text{La}_2\text{Zr}_2\text{O}_7$ and La_2O_3 can provide good passivation. However, these decomposition phases are poor ionic conductors, which give rise to high interfacial resistance. Therefore, the application of coating layers is also recommended between LLZO and the cathode to reduce interfacial resistance. The introduction of Nb oxides at cathode interfaces is recently demonstrated to effectively reduce the interfacial resistance.^[42,44]

In addition to the electrochemical decomposition of the solid electrolyte itself at the interfaces with electronically conductive additives (e.g., carbon), the presence of the active material in a real all-solid-state cell may also induce the electrochemical decomposition of the solid electrolyte. Therefore, the effect of the active material on the thermodynamic electrochemical stability of solid electrolytes should also be considered. Given the conventional understanding about that the high interfacial resistance caused by the chemical incompatibility between solid electrolyte and active material during high-temperature sintering process and/or room-temperature charge/discharge processes, our work provides unprecedented insight for the understanding of the interfacial resistances in all-solid-state lithium ion batteries.

4. Conclusion

In summary, the thermodynamic stability windows and decomposition phase equilibria of LGPS and LLZO were calculated using the first principles computation method. A Li/electrolyte/electrolyte-carbon cell was proposed to replace current Li/electrolyte/Pt semiblocking electrode to obtain the intrinsic stability window of the solid electrolytes. The reduction and oxidation of both LGPS and LLZO are confirmed by the new CV scans and the XPS results. The results indicate that both solid electrolytes have significantly narrower electrochemical window than previously reported apparent window based on the semiblocking electrode. Therefore, the high interfacial resistances arising from the decomposition of solid electrolyte should be addressed by stabilizing the solid electrolyte. Extending the stability window of the solid electrolytes through the spontaneous formation or artificial application of SEI layers is the key to good performance of the bulk-type all-solid-state lithium ion batteries.

5. Experimental Section

Synthesis: Polycrystalline $\text{Li}_{10}\text{GeP}_2\text{S}_{12}$ powder was prepared with the same method reported elsewhere.^[2] A Ta-doped cubic garnet compound with the composition of $\text{Li}_{6.75}\text{La}_3\text{Zr}_{1.75}\text{Ta}_{0.25}\text{O}_{12}$ was prepared through solid state reaction. Starting materials of $\text{LiOH}\cdot\text{H}_2\text{O}$ (99.995%, Sigma

Aldrich), $\text{La}(\text{OH})_3$ (99.9%, Sigma Aldrich), ZrO_2 (99.99%, Sigma Aldrich), Ta_2O_5 (99.99%, Sigma Aldrich), were weighed and mixed based on the stoichiometric ratio. 10% excess $\text{LiOH}\cdot\text{H}_2\text{O}$ was used to compensate the Li loss during high-temperature calcinations and sintering. The mixture was ball-milled (PM 100, Retsch) in 2-propanol for 24 h with zirconia balls in a zirconia vial, and then dried, heated in air at 950 °C for 12 h. The ball-milling and heating were repeated once to enhance purity. The collected powder samples were pressed into pellets under isostatic pressure (120 MPa). The pellet was fully covered with powder with the same composition and sintered in air at 1230 °C for 12 h in a MgO crucible. The residual powder samples were transferred to the Ar-filled glovebox to protect its slow reaction with the $\text{H}_2\text{O}/\text{CO}_2$ in air. For the preparation of the carbon-coated LLZO particles, the as-prepared LLZO powder was ground using a high-energy vibrating mill (SPEX SamplePrep* 8000M Mixer/Mill) for 1 h (to reduce its particle size), dispersed into a solution of polyvinylpyrrolidone (10 wt% in ethanol), and then vigorously stirred for 30 min. The product was then dried and sintered at 700 °C for 1 h in argon flow to enable carbon coating.

Characterization: Powder X-ray diffraction patterns were obtained with a D8 Advance with LynxEye and SolX (Bruker AXS, WI, USA) using $\text{Cu K}\alpha$ radiation. The morphologies of the sample were examined using a Hitachi SU-70 field-emission scanning electron microscope and JEOL 2100F field emission transmission electron microscope (TEM). The surface chemistry of the samples was examined by X-ray photoelectron spectroscopy (XPS) using a Kratos Axis 165 spectrometer. To prepare the sample for XPS test, LLZO electrodes were charged or discharged to a certain voltage in a liquid electrolyte using a Swagelok cell, and held at that voltage for 24 h. The electrodes were then taken out from the cell, and rinsed by dimethyl carbonate (DMC) inside the glove box for three times. All samples were dried under vacuum overnight, placed in a sealed bag, and then transferred into the XPS chamber under inert conditions in a nitrogen-filled glove bag. Ar^+ sputtering was performed for 2 h (0.5 h per step) until the carbon and/or SEI layer on the surface of the LLZO electrodes are removed. XPS data were collected using a monochromated Al $\text{K}\alpha$ X-ray source (1486.7 eV). The working pressure of the chamber was lower than 6.6×10^{-9} Pa. All reported binding energy values are calibrated to the C 1s peak at 284.8 eV.

Electrochemistry: 120 mg LGPS powder was pressed into a pellet (diameter 13 mm; thickness 2 mm) under isostatic pressure (120 MPa) in an Ar atmosphere. It was then sputtered with Pt on one side and attached with Li metal on the other side to make the Li/LGSPS/Pt cell. To make the Li/LGSPS/LGPS-C cell, 10 mg LGPS-C powder (LGPS: graphite is 75:25 in weight) was put on the top of 120 LGPS powder and then cold-pressed together under 360 MPa, while Li metal was attached on the other side of LGPS pellet. The cyclic voltammograms of the Li/LGPS/Pt and Li/LGPS/LGPS-C cells were measured with a scan rate of 0.1 mV s^{-1} . The LLZO electrodes were prepared by mixing the carbon-coated LLZO and carbon black (weight ratio of carbon-coated LLZO to carbon is 40:60) by hand-grinding in the mortar, and mixing with 10 wt% polyvinylidene fluoride (PVDF) and *n*-methylpyrrolidone (NMP) to make the electrode slurry. The electrodes were prepared by casting the electrode slurry onto copper or aluminum foils and dried at 120 °C overnight. The loading of the active material on each electrode is about 1 mg. The charge/discharge tests of the LLZO electrodes were carried out in Swagelok cells using Li metal as the counter electrode and 1M LiPF_6 in a mixed solvent of FEC, HFE, and FEMC (volume ratio is 2:6:2) as the liquid electrolyte. To make the Li/LLZO/LLZO-C cell for the electrochemical stability window test, the LLZO electrode slurry was coated on the top surface of LLZO pellet, dried at 120 °C overnight, and then sputtered with Pt to improve the electrical contact. After that, Li metal was attached on the other side of the pellet and cured at 200 °C to enhance the interfacial contact between Li and LLZO. The cyclic voltammogram of the Li/LLZO/LLZO-C cell was tested with a scan rate of 0.01 mV s^{-1} . The charge/discharge behavior was tested using an Arbin BT2000 workstation at room temperature. The cyclic voltammetry measurements were carried on an electrochemistry workstation (Solartron 1287/1260).

First Principles Computation Methods: All density functional theory (DFT) calculations in the work were performed using the Vienna Ab

initio Simulation Package (VASP) within the projector augmented-wave approach, and the Perdew–Burke–Ernzerhof (PBE) generalized gradient approximation (GGA) functional was used. The DFT parameters were consistent with the parameters used in Materials Project (MP).^[45] The crystal structures of LGPS and LLZO were obtained from the ICSD database and ordered using pymatgen if the material has disordering sites. The electrochemical stability of the solid electrolyte materials was studied using the grand potential phase diagrams constructed using pymatgen,^[46] which identify the phase equilibria of the material in equilibrium with an opening Li reservoir of Li chemical potential μ_{Li} . As in the previous studies,^[16,47] the applied potential ϕ was considered in the Li chemical potential μ_{Li} as

$$\mu_{\text{Li}}(\phi) = \mu_{\text{Li}}^0 - e\phi \quad (1)$$

where μ_{Li}^0 is the chemical potential of Li metal, and the potential ϕ is referenced to Li metal.

Supporting Information

Supporting Information is available from the Wiley Online Library or from the author.

Acknowledgements

F.H. and Y.Z. contributed equally to this work. The authors thank Dr. Karen J. Gaskell at the Surface Analysis Center of University of Maryland for the help on the XPS data analysis. The authors thank Dr. Kang Xu at the U.S. Army Research Laboratory for providing the high-voltage liquid electrolyte. C.W. and F.H. thank the support from National Science Foundation under Award No. 1235719 and Army Research Office (Program Manager: Dr. Robert Mantz), under Award No. W911NF1510187. Y.M. and Y.Z. thank the support from U.S. Department of Energy, Office of Energy Efficiency and Renewable Energy, under Award No. DE-EE0006860, and the computational facilities from the University of Maryland supercomputing resources and from the Extreme Science and Engineering Discovery Environment (XSEDE) supported by National Science Foundation Award No. TG-DMR130142.

Received: August 9, 2015

Revised: December 21, 2015

Published online: January 21, 2016

- [1] V. Thangadurai, S. Narayanan, D. Pinzaru, *Chem. Soc. Rev.* **2014**, *43*, 4714.
- [2] N. Kamaya, K. Homma, Y. Yamakawa, M. Hirayama, R. Kanno, M. Yonemura, T. Kamiyama, Y. Kato, S. Hama, K. Kawamoto, A. Mitsui, *Nat. Mater.* **2011**, *10*, 682.
- [3] S. Ohta, T. Kobayashi, T. Asaoka, *J. Power Sources* **2011**, *196*, 3342.
- [4] A. Sakuda, A. Hayashi, M. Tatsumisago, *Chem. Mater.* **2009**, *22*, 949.
- [5] F. Han, T. Gao, Y. Zhu, K. J. Gaskell, C. Wang, *Adv. Mater.* **2015**, *27*, 3473.
- [6] J. Haruyama, K. Sodeyama, L. Han, K. Takada, Y. Tateyama, *Chem. Mater.* **2014**, *26*, 4248.
- [7] T. Kobayashi, A. Yamada, R. Kanno, *Electrochim. Acta* **2008**, *53*, 5045.
- [8] M. J. G. Jak, M. S. Pontfoort, N. Van Landschoot, A. S. Best, E. M. Kelder, D. R. MacFarlane, M. Forsyth, J. Schoonman, *Solid State Ionics* **2001**, *143*, 57.
- [9] J. E. Trevey, K. W. Rason, C. R. Stoldt, S. H. Lee, *Electrochem. Solid State Lett.* **2010**, *13*, A154.

- [10] A. Aboulaich, R. Bouchet, G. Delaizir, V. Seznec, L. Tortet, M. Morcrette, P. Rozier, J. M. Tarascon, V. Viallet, M. Dolle, *Adv. Energy Mater.* **2011**, *1*, 179.
- [11] S. Ohta, S. Komagata, J. Seki, T. Saeki, S. Morishita, T. Asaoka, *J. Power Sources* **2013**, *238*, 53.
- [12] N. Ohta, K. Takada, L. Q. Zhang, R. Z. Ma, M. Osada, T. Sasaki, *Adv. Mater.* **2006**, *18*, 2226.
- [13] R. B. Cervera, N. Suzuki, T. Ohnishi, M. Osada, K. Mitsuishi, T. Kambara, K. Takada, *Energy Environ. Sci.* **2014**, *7*, 662.
- [14] J. B. Goodenough, Y. Kim, *Chem. Mater.* **2009**, *22*, 587.
- [15] A. Schwöbel, R. Hausbrand, W. Jaegermann, *Solid State Ionics* **2015**, *273*, 51.
- [16] Y. Mo, S. P. Ong, G. Ceder, *Chem. Mater.* **2012**, *24*, 15.
- [17] J. B. Bates, N. J. Dudney, B. Neudecker, A. Ueda, C. D. Evans, *Solid State Ionics* **2000**, *135*, 33.
- [18] M. Tatsumisago, F. Mizuno, A. Hayashi, *J. Power Sources* **2006**, *159*, 193.
- [19] M. Tatsumisago, A. Hayashi, *Solid State Ionics* **2012**, *225*, 342.
- [20] B. R. Shin, Y. J. Nam, D. Y. Oh, D. H. Kim, J. W. Kim, Y. S. Jung, *Electrochim. Acta* **2014**, *146*, 395.
- [21] Y. Zhu, X. He, Y. Mo, *ACS Appl. Mater. Interfaces* **2015**, *7*, 23685.
- [22] E. Rangasamy, Z. Liu, M. Gobet, K. Pilar, G. Sahu, W. Zhou, H. Wu, S. Greenbaum, C. Liang, *J. Am. Chem. Soc.* **2015**, *137*, 1384.
- [23] S. Ujiie, A. Hayashi, M. Tatsumisago, *Solid State Ionics* **2012**, *211*, 42.
- [24] H. M. Chen, C. Maohua, S. Adams, *Phys. Chem. Chem. Phys.* **2015**, *17*, 16494.
- [25] V. Thangadurai, D. Pinzaru, S. Narayanan, A. K. Baral, *J. Phys. Chem. Lett.* **2015**, *6*, 292.
- [26] L. Cheng, E. J. Crumlin, W. Chen, R. Qiao, H. Hou, S. Franz Lux, V. Zorba, R. Russo, R. Kostecki, Z. Liu, K. Persson, W. Yang, J. Cabana, T. Richardson, G. Chen, M. Doeff, *Phys. Chem. Chem. Phys.* **2014**, *16*, 18294.
- [27] Y. Wang, W. Lai, *J. Power Sources* **2015**, *275*, 612.
- [28] M. Kotobuki, H. Munakata, K. Kanamura, Y. Sato, T. Yoshida, *J. Electrochem. Soc.* **2010**, *157*, A1076.
- [29] Y. Wang, A. Huq, W. Lai, *Solid State Ionics* **2014**, *255*, 39.
- [30] S. Toda, K. Ishiguro, Y. Shimonishi, A. Hirano, Y. Takeda, O. Yamamoto, N. Imanishi, *Solid State Ionics* **2013**, *233*, 102.
- [31] F. Tietz, T. Wegener, M. T. Gerhards, M. Giarola, G. Mariotto, *Solid State Ionics* **2013**, *230*, 77.
- [32] I. Bespalov, M. Datler, S. Buhr, W. Drachsel, G. Rupprechter, Y. Suchorski, *Ultramicroscopy* **2015**, *159*, 147.
- [33] K. Ishiguro, Y. Nakata, M. Matsui, I. Uechi, Y. Takeda, O. Yamamoto, N. Imanishi, *J. Electrochem. Soc.* **2013**, *160*, A1690.
- [34] R. Sudo, Y. Nakata, K. Ishiguro, M. Matsui, A. Hirano, Y. Takeda, O. Yamamoto, N. Imanishi, *Solid State Ionics* **2014**, *262*, 151.
- [35] L. Cheng, W. Chen, M. Kunz, K. Persson, N. Tamura, G. Chen, M. Doeff, *ACS Appl. Mater. Interfaces* **2015**, *7*, 2073.
- [36] J. Wolfenstine, J. L. Allen, J. Read, J. Sakamoto, *J. Mater. Sci.* **2013**, *48*, 5846.
- [37] U. v. Alpen, A. Rabenau, G. H. Talat, *Appl. Phys. Lett.* **1977**, *30*, 621.
- [38] G. Nazri, *Solid State Ionics* **1989**, *34*, 97.
- [39] S. Wenzel, T. Leichtweiss, D. Krüger, J. Sann, J. Janek, *Solid State Ionics* **2015**, *278*, 98.
- [40] P. Hartmann, T. Leichtweiss, M. R. Busche, M. Schneider, M. Reich, J. Sann, P. Adelhelm, J. Janek, *J. Phys. Chem. C* **2013**, *117*, 21064.
- [41] Y. Yang, G. Zheng, Y. Cui, *Chem. Soc. Rev.* **2013**, *42*, 3018.
- [42] N. Ohta, K. Takada, I. Sakaguchi, L. Zhang, R. Ma, K. Fukuda, M. Osada, T. Sasaki, *Electrochem. Commun.* **2007**, *9*, 1486.
- [43] S. Visco, Y. Nimon, B. Katz, L. De Jonghe, N. Goncharenko, V. Loginova, WO Patent 2,013,074,772, **2013**.
- [44] T. Kato, T. Hamanaka, K. Yamamoto, T. Hirayama, F. Sagane, M. Motoyama, Y. Iriyama, *J. Power Sources* **2014**, *260*, 292.
- [45] A. Jain, G. Hautier, C. J. Moore, S. Ping Ong, C. C. Fischer, T. Mueller, K. A. Persson, G. Ceder, *Comput. Mater. Sci.* **2011**, *50*, 2295.
- [46] S. P. Ong, L. Wang, B. Kang, G. Ceder, *Chem. Mater.* **2008**, *20*, 1798.
- [47] S. P. Ong, Y. Mo, W. D. Richards, L. Miara, H. S. Lee, G. Ceder, *Energy Environ. Sci.* **2013**, *6*, 148.